Calcium/chitosan spheres as catalyst for biodiesel production

Leandro Marques Correia, Natalia de Sousa Campelo, Raquel de Freitas Albuquerque, Celio Loureiro Cavalcante, Juan Antonio Cecilia, Enrique Rodriguez-Castellon, Eric Guibal, Rodrigo Silveira Vieira

Calcium/chitosan spheres as catalyst for biodiesel production

Leandro Marques Correia,[a] Natália de Sousa Campelo,[a] Raquel de Freitas Albuquerque,[a] Célio Loureiro Cavalcante Jr,[a] Juan Antonio Cecilia,[b] Enrique Rodríguez-Castellón,[b] Eric Guibal[c] and Rodrigo Silveira Vieira[a]*

Abstract

Chitosan, an abundant biopolymer extracted from crustacean shells, can be used as a structuring agent by the insertion of calcium oxide and used as a catalyst in transesterification reactions. These calcium-incorporated chitosan spheres were calcined in order to obtain a porous calcium catalyst without organic material. The materials were characterized using X-ray diffraction, thermogravimetric analysis, Fourier transform infrared and X-ray photoelectron spectroscopies, temperature-programmed desorption of CO_2, scanning electron microscopy and specific surface area analysis. Afterwards the calcined calcium/chitosan spheres were used in the transesterification reaction of sunflower oil with methanol. The conversion of sunflower oil to methyl esters (Y_{FAME}), under optimized reaction conditions, which were determined by factorial experimental design (X_{MR}, 1:9; X_{CAT}, 3 wt%; time, 4 h; temperature, °60 C; magnetic stirring, 1000 rpm), was 56.12 ± 0.32 wt%. These results show that chitosan can be used as a precursor for the formation of calcium/chitosan spheres, yielding a porous calcium oxide (with higher surface area) that can be used as an alkaline catalyst for biodiesel production.

Keywords: chitosan; calcium oxide; transesterification reaction; methyl esters

INTRODUCTION

Biodiesel is a mixture of alkyl esters, such as methyl, ethyl or propyl esters, of long-chain fatty acids produced from renewable sources like refined vegetable oil (in oil seed plants) and animal fats.[1] Its primary application is the replacement of fossil fuel in diesel engines; it is comparable with petroleum diesel in almost all its properties. Biodiesel also presents several advantages compared to fossil fuel: biodegradable, non-toxic and renewable[2] and free of sulfur and aromatics.[3] In addition, its use contributes to reducing emissions of carbon monoxide and aromatic hydrocarbons,[4] and to increasing the lubricity of motor engines.[5] Nevertheless, its main disadvantage is its high production cost, which is possibly due to the price of feedstocks and/or the type of catalysts used in its production.[6]

There is an increasing interest in the possibility of replacing the homogeneous alkaline hydroxides, carbonates or metal alkoxides with heterogeneous solid catalysts that should be insoluble in methanol.[7] These heterogeneous catalysts have some advantages: they are environmentally friendly, they do not induce corrosion or emulsion, and they present fewer control problems.[8] They are also much easier to separate from products and they can be designed to give better activity, selectivity and longer catalyst lifetimes.[9] Another important factor is the possibility of storing the catalysts and guarantee their catalytic activity for immediate use.

Many types of these catalysts have been reported in the literature for biodiesel production. Examples include metal oxide,[10] doped metal oxide,[11] supported catalyst,[12] zeolites,[13,14] hydrotalcites,[15,16] organics bases[17] and ion-exchange resin.[18]

Chitosan is a biopolymer obtained by alkaline deacetylation of chitin[19,20] that is found especially in the skeleton of marine invertebrates, insects, some algae and mucoraceous fungi.[21] Its characteristics, such as non-toxicity, biocompatibility and biodegradability,[19,20] have attracted the attention of researchers for its use in various applications such as an adsorbent, catalyst and support material. Furthermore, its high sorption capacities, the stability of metal ions on its structure and the physical (and chemical) versatility of the biopolymer are some of the reasons for the increasing interest in using it for supporting catalytic metals.[22] The presence of hydroxyl and amino groups imparts a very high chemical reactivity to the polymer.[23] One of the most interesting advantages of chitosan is its versatility: it can be obtained in various physical forms such as powder,[24] flakes (or spheres),[24] gel spheres,[22,24] membranes,[24,25] fibres[24,26] and sponges.[27]

* *Correspondence to: Rodrigo Silveira Vieira, Grupo de Pesquisa em Separações por Adsorção (GPSA), Departamento de Engenharia Química, Universidade Federal do Ceará – UFC, Campus do Pici, Bl. 709, 60455-760, Fortaleza-CE, Brazil. E-mail: rodrigo@gpsa.ufc.br*

a *Grupo de Pesquisa em Separações por Adsorção (GPSA), Departamento de Engenharia Química, Universidade Federal do Ceará – UFC, Campus do Pici, Bl. 709, 60455-760 Fortaleza-CE, Brazil*

b *Departamento de Química Inorgánica, Facultad de Ciencias, Universidad de Málaga, Campus de Teatinos, 29071 Málaga, Spain*

c *Ecole des Mines d'Alès, Centre des Matériaux des Mines d'Alès, 6 Avenue de Clavières, F-30319 Ales Cedex, France*

Among the oxides of alkaline earth metals, calcium oxide is the most widely used inorganic catalyst for transesterification reactions because of its relatively high basic strength and low environmental impact (due to its low solubility in methanol). It can be synthesized from cheap sources such as limestone and calcium hydroxide,[28] and used as a catalyst either in pure form of $CaCO_3$, $Ca(OH)_2$ and CaO, or supported on various materials such as alumina,[29] mesoporous silica[30] and chitosan.[31]

Various heterogeneous CaO-based solid catalysts have been investigated for biodiesel production: silica-supported tin oxides,[32] $Ca_xMg_{2-x}O_2$,[33] lipase immobilized on magnetic chitosan microspheres,[34] calcium-supported tin oxides,[35] $CaO-MoO_3-$SBA-15,[36] Cu(II) and Co(II) supported on chitosan,[37] magnesium oxide immobilized on chitosan[38] and CaO immobilized on chitosan beads,[12] eggshell and crab shell.[39]

There are some reports in the literature of using chitosan as a support for metal ion impregnation and its application in transesterification reactions for biodiesel production. Silva *et al.*[37] described biodiesel synthesis from babassu and soybean oils using a heterogeneous catalyst with Cu(II) and Co(II) adsorbed on chitosan, where it was possible to reach biodiesel conversion in the range 70–90 wt%. Almerindo *et al.*[38] prepared a catalyst based on magnesium oxide immobilized on chitosan for biodiesel production using the transesterification reaction of soybean oil with ethanol, and the yields of ethyl esters ranged between 30 and 75 wt%. Fu *et al.*[12] described the synthesis of a catalyst by immobilization of CaO onto chitosan beads and its use as a heterogeneous catalyst to produce biodiesel, through transesterification of soybean oil with methanol; high levels of conversion were obtained (up to 97 wt%). Those authors used two different analytical techniques (SEM and XRD); however, they did not correlate the catalytic characteristics with the biodiesel production, in order to determine if $CaCO_3$ was converted to $Ca(OH)_2$ and CaO. Kayser *et al.*[40] described the synthesis of a chitosan–cryogel catalyst for biodiesel production, using triolein and soybean oil with methanol for transesterification reactions, obtaining biodiesel yields of up to 90% in 8–32 h at 100–150 °C.

The objective of the study reported here was (a) to characterize the metal oxide obtained from the calcination of calcium-incorporated chitosan spheres and (b) to evaluate the catalytic properties for the transesterification of sunflower oil with methanol. The advantages of the use of calcium/chitosan spheres as a heterogeneous catalyst for biodiesel production are the low cost of chitosan and as directional structure agent having a higher surface area than pristine calcium oxide. The material was characterized using XRD, thermogravimetric analysis (TGA/DTG), Fourier transform infrared (FTIR) spectroscopy, X-ray photoelectron spectroscopy (XPS), temperature-programmed desorption of CO_2 (CO_2-TPD), SEM and adsorption/desorption of nitrogen, in order to evaluate the conversion of calcium carbonate into calcium oxide and the structural modification of the catalyst. The influences of X_{MR} (molar ratio) and X_{CAT} (catalyst amount) on the conversion of sunflower oil to methyl esters (Y_{FAME}, wt%) were investigated. A factorial design process was used for the optimization of experimental conditions.

MATERIALS AND METHODS

Materials and reagents

Chitosan (with a degree of deacetylation of 85%, determined using potentiometric titration) was obtained from Polymar (Brazil). Commercial-grade sunflower oil (Liza, Brazil) was obtained from a local supermarket. The properties of sunflower oil are described elsewhere.[34] Methanol (99.50%) was supplied by Vetec (Brazil). The gases used in the experiments were He and CO_2 (99.99%), supplied by Air Liquide (Brazil). Methyl heptadecanoate (99.99% purity) was obtained from Sigma (USA). The fatty acid composition of sunflower oil was initially determined by promoting the esterification of a sample, followed by quantification of methyl esters using gas chromatography. This reaction was carried out according to the procedure described in the ISO standard 15304:2002 (E).[41]

Synthesis and activation of material

A 5 wt% chitosan solution, prepared in concentrated acetic acid (5 mL/100 mL), was mixed, under vigorous stirring, with $Ca(NO_3)_2 \cdot 4H_2O$ respecting the monomer-to-metal ratio of 1:1. The chitosan/calcium solution was added dropwise into 50 mL/100 mL of 35% (v/v) aqueous ammonia solution to produce calcium/chitosan spheres. The composite hydrogels remained in the solution for 24 h for neutralization at pH = 7, before being repeatedly washed with distilled water followed by drying at room temperature. Before the calcium/chitosan spheres could be used as a catalyst, they needed to be activated thermally by heating the material in a muffle oven up to 900 °C for 1 h at a heating rate of 5 °C min^{-1}. During this calcination, the organic material was eliminated and porous spheres (based on calcium oxide) were formed.

Characterization of material

The calcium/chitosan spheres were characterized using XRD, TGA/DTG, FTIR spectroscopy, XPS, CO_2-TPD, SEM and nitrogen adsorption/desorption isotherms, both before and after calcination, to identify the differences in the properties and characteristics of the various materials during the synthesis process.

XRD was performed using an X'Pert Pro MPD diffractometer with Co Kα radiation ($\lambda = 1.788965$ Å) operating at a voltage of 40 kV and a current of 40 mA. To perform the analysis, sample powders were placed in the cavity of the support used as the sample holder. The spectra were obtained by sweeping in the range 10–70° at a scan rate of 0.5° min^{-1}.

Thermal decomposition of the catalysts was evaluated using TGA/DTG with a Shimadzu TGA-50 analyser. The following conditions were used: air flow, 50 mL min^{-1}; heating rate, 10 °C min^{-1}; temperature, from room temperature (25 °C) to 1000 °C.

FTIR spectra of the samples were recorded with a Shimadzu FTIR-8500 spectrometer in the range 600–4000 cm^{-1}. A standard KBr technique was used for preparing the samples. The XPS measurements were carried out with a Physical Electronics 5700 spectrometer, using a Mg Kα source (1253.6 eV; model 04–548 dual anode X-ray source).

The alkalinity of the catalyst was studied using CO_2-TPD. Approximately 100 mg of each sample was pretreated with a stream of helium at 800 °C for 30 min (10 °C min^{-1} and 60 mL min^{-1}). The reaction temperature was then decreased to 100 °C, and a flow of pure CO_2 (60 mL min^{-1}) was subsequently introduced into the reactor for 30 min. The CO_2-TPD reaction was carried out between 100 and 800 °C under a flow of helium (10 °C min^{-1}, 30 mL min^{-1}). The amount of CO_2 evolved was analysed using a quadrupole mass spectrometer (Balzer GSB 300 02) equipped with a Faraday detector (0–200 U), which monitored the mass of CO_2 (44 U) during the experiment.

SEM images of the samples were obtained using a JEOL JXA-840A (Japan) scanning electron microscope (20 kV) under a

vacuum of 1.33×10^{-6} mbar (1.33×10^{-4} Pa). Prior to analysis the samples were coated with a thin layer of gold (10 nm) using a sputter coater (SCD 050, Bal-Tec, Liechtenstein).

The surface area, pore diameter and pore volume were determined using nitrogen adsorption/desorption isotherms, according to the BET method. Nitrogen isotherms were measured at −196 °C using a Quantachrome Autosorb-1 MP analyser.

Transesterification reaction

The transesterification reaction was conducted in a three-necked glass batch reactor with a condenser and magnetic stirrer. This reaction was carried out by mixing 10 mL of sunflower vegetable oil with different volumes of methanol (X_{MR} = 1:6; 1:9 and 1:12) and different amounts of catalyst (X_{CAT} = 1, 2 and 3 wt%). The temperature was fixed at 60 °C and the time was set to 4 h. The catalyst was separated by centrifuging the sample at 2250 rpm for 20 min, and the reaction mixture (sunflower oil reacted to methyl esters and glycerin) was placed in a funnel for phase separation. The residual methanol was evaporated using a rotary evaporator at 100 °C.

Determination of biodiesel using gas chromatography

The content of methyl esters was determined according to the procedure described in standard EN 14103.[42] Analyses were done using a Varian CP-3800 gas chromatograph equipped with a CP-WAX 52CB (30 m × 0.25 mm × 0.05 μm) capillary column and a flame ionization detector. For sample preparation, 250 mg of ester phase to be analysed was added to 5 mL of a solution containing methyl heptadecanoate (at a final concentration of 10 mg L^{-1}, serving as internal standard) in heptane. The mixture was gently stirred (to prevent degassing) and then 1 μL was injected into the chromatograph. The content of biodiesel was calculated according to

$$Y_{FAME}\ (\text{wt}\%) = \left(\frac{\sum A_t - A_{pi}}{A_{pi}} \right) \frac{C_{pi} \times V_{pi} \times 100}{W} \qquad (1)$$

where $\sum A_t$ is the total area of the peaks of methyl esters; A_{pi} is the peak area of internal standard (methyl heptadecanoate); C_{pi} is the concentration of internal standard solution (10 mg L^{-1}); V_{pi} is the added volume in 5 mL solution of methyl heptadecanoate; and W is the weight of the sample (i.e. 250 mg).

Experimental design

The experimental design was carried out through nine transesterification tests. Some experimental parameters were kept constant (temperature, time and magnetic stirring) and X_{MR} (molar ratio of oil to alcohol, mol/mol) and X_{CAT} (catalyst amount, wt%) were selected as operating variables. The conversion of sunflower oil to methyl esters (Y_{FAME}, wt%) was optimized using a 3^2 Box-Behnken design model with the two coded variables X_{MR} and X_{CAT}. The results were evaluated by analysing the response surface, using STATISTICA 7.0 software, with a confidence interval of 95%. Table 1 describes the factors and the levels of response conversion of sunflower oil to methyl esters (Y_{FAME}), selected for this experimental design plan with its central point of experimental planning, performed in triplicate to check the reproducibility of results.

Table 1. Experimental design for biodiesel production

Variable	Coded symbol	Coded level −1	0	1
Molar ratio of sunflower oil to methanol	X_{MR} (mol/mol)	1:6	1:9	1:12
Catalyst amount	X_{CAT} (wt%)	1	2	3

RESULTS AND DISCUSSION

Characterization of material

XRD analysis

The XRD patterns of chitosan, calcium/chitosan spheres and calcium/chitosan spheres calcined at 900 °C for 1 h are shown in Figs 1(a)–(c), respectively. For chitosan (Fig. 1(a)) two peaks are observed at $2\theta = 11.1°$ and 23.1°. The second peak is related to the deformation of the amorphous material.[43] For calcium/chitosan spheres (Fig. 1(b)) the four peaks observed at $2\theta = 11.9°$, 23.0°, 29.2° and 34.4° correspond to peaks of $CaCO_3$. The pattern of the calcined calcium/chitosan spheres shows the formation of a mixed crystalline material of CaO, $Ca(OH)_2$ and $CaCO_3$ with peaks at $2\theta = 21.1°$, 24.5°, 26.9°, 33.2°, 34.9°, 40.0°, 42.0°, 43.9°, 46.1°, 48.2°, 50.4°, 55.5°, 59.8° and 64.3° (Fig 1(c)).

TGA/DTG analysis

TGA/DTG curves of calcium/chitosan spheres are shown in Fig. 2. Two mass losses were observed at different temperatures. The first one (45.5 wt%) occurs in the temperature range 50–235 °C. This can be attributed to the decomposition of organic material, referring to removal or oxidation of chitosan polymer.[44] The second mass loss (24.5 wt%) occurs in the range 250–600 °C, and is associated with the transformation of $Ca(NO_3)_2 \cdot 4H_2O$ to CaO.[45]

FTIR analysis

The absorption spectra in the infrared region between 4000 and 400 cm^{-1} are displayed in Fig. 3 for chitosan, calcium/chitosan spheres and calcined calcium/chitosan spheres. Bands near 3400 cm^{-1} are observed for all samples: they correspond to hydroxyl stretching vibration. For pristine chitosan a small band appeared at (a) 2887 cm^{-1} due to the (—CH_2) stretching mode and (b) 1664 cm^{-1} attributed to axial strain of amide (C═O) group in remaining acetyl groups. The angular deformation of amino group is observed at 1592 cm^{-1} and the axial deformation of amide group (C—N) is identified at 1415 cm^{-1}. There is a symmetric angular deformation (—CH_3) at 1378 cm^{-1}, while the axial deformation of (—CN) groups in amino moieties appears around 1070 cm^{-1}. The similarity between Figs 3(a) and (b) indicates that there are amino and hydroxyl groups available. In this case not all the amino and hydroxyl groups are complexed with calcium ions. The spectrum of spheres after calcination (Fig. 3(c)) shows the appearance of a band at 3643 cm^{-1}, which is attributed to $Ca(OH)_2$. The bands at 1417 and 875 cm^{-1} are associated with the stretching of CO_3^{2-}, and the band of inorganic calcium oxide appears at 500 cm^{-1}.

XPS analysis

XPS is a very useful tool for determining the composition of the surface of the catalyst and the chemical state of its constituents. In

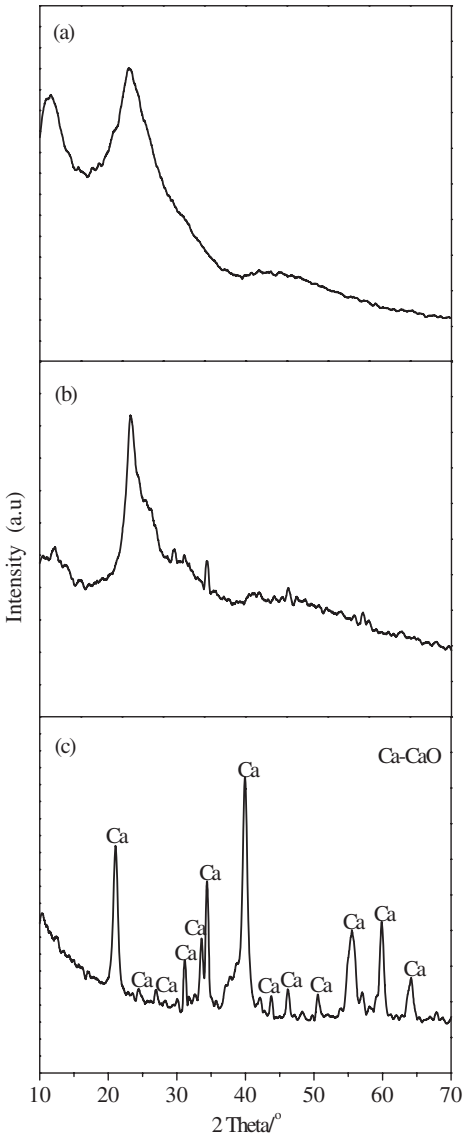

Figure 1. XRD patterns of (a) chitosan, (b) calcium/chitosan spheres and (c) calcined calcium/chitosan spheres.

Table 2, the binding energy values and the atomic concentration of the elements for the different materials are reported. The surface concentration of Ca is lower for chitosan/calcium spheres (1.62%) than for calcined chitosan/calcium spheres (16.65%). The C 1 s signal for chitosan/calcium spheres can be decomposed into four contributions at 284.8 eV (73%), 286.3 eV (19%), 287.7 eV (5%) and 288.5 eV (3%). The contribution at low binding energy is assigned to carbons from chitosan and adventitious contamination, and the others at higher binding energies to carbon bonded to oxygen and nitrogen atoms. The C 1 s signal is totally changed after calcination and a very intense contribution at 289.5 eV (63%) appears. This contribution is assigned to the presence of calcium carbonate on the surface. Then the percentage of C (atomic concentration) as carbonate is $(25.38 \times 63)/100 = 15.98\%$. This value is very near to that found for Ca (16.65%) indicating that calcium is mainly on the surface as carbonate. Upon calcination, the percentage of nitrogen is practically zero. The binding energy for S $2p_{3/2}$ (167.7 eV) is typical of S(VI). The results of XPS are in accordance with the XRD results, for which were observed mainly peaks for $CaCO_3$.

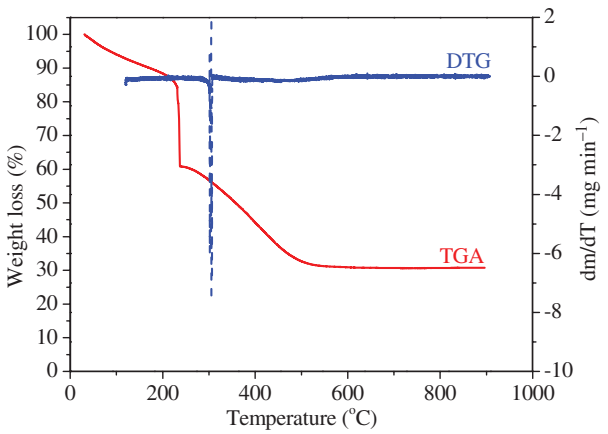

Figure 2. TGA-DTG curves of calcium/chitosan spheres.

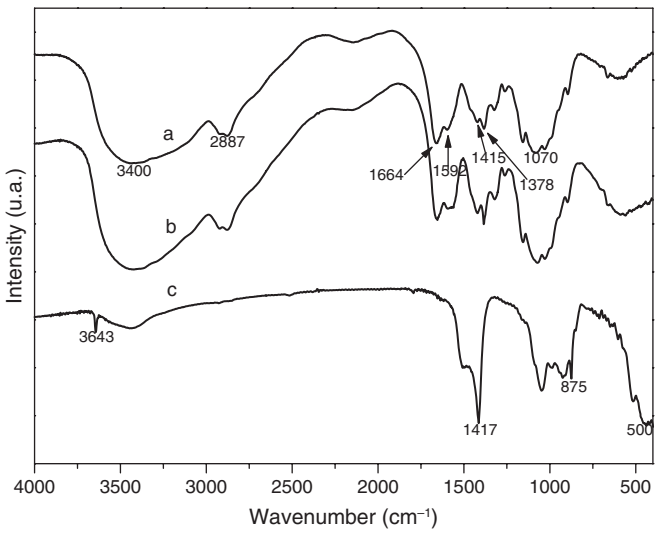

Figure 3. FTIR spectra of (a) chitosan, (b) calcium/chitosan spheres and (c) calcined calcium/chitosan spheres.

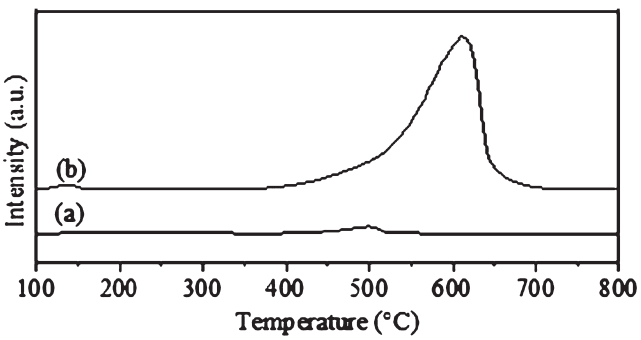

Figure 4. CO_2-TPD curves of (a) calcium/chitosan spheres and (b) calcined calcium/chitosan spheres.

CO_2-TPD analysis

The alkalinity of the catalyst was studied using by CO_2-TPD (Fig. 4). In the case of the calcined material two peaks are observed. The first one is located between 100 and 386 °C and the other more intense and well-defined peak between 386 and 710 °C. This result indicates that the presence of strong alkaline sites on the $CaCO_3$ surface, as a major part of total alkaline sites, is due to the

Table 2. Binding energy (BE) of the constituents of chitosan/calcium spheres before and after calcination and their atomic concentration (AC) determined using XPS

	Chitosan/calcium spheres		Calcined chitosan/calcium spheres	
Element	BE (eV)	AC (%)	BE (eV)	AC (%)
C 1 s	284.7(73%)	75.99	284.7(31%)	25.38
	286.3(19%)		287.4(6%)	
	287.7(5%)		289.5(63%)	
	288.5(3%)			
N 1 s	398.8	3.24	398.8	0.05
O 1 s	530.4(17%)	18.89	531.4	57.89
	532.3(83%)			
S $2p_{3/2}$	167.7	0.26	167.7	0.02
Ca $2p_{3/2}$	347.1	1.62	347.1	16.65

desorption of CO_2 from calcium carbonates that takes place at high temperatures.[39]

SEM analysis

An SEM image of calcium/chitosan spheres is shown in Fig. 5(a). The calcium/chitosan spheres are roughly spherical before calcination. After calcination (Fig. 5(b)), the spheres lose their mechanical strength and are disintegrated (shape loss), with an apparent porous structure (formation of porous CaO).

Texture analysis

The nitrogen adsorption/desorption isotherms of calcium/chitosan spheres and calcined calcium/chitosan spheres are described in the supporting information (Fig. AM1). Type IV isotherms are obtained for calcined calcium/chitosan spheres. In accordance with the IUPAC classification, this is characteristic of macroporous materials: H1 type is representative of a material with a narrow and uniform pore size distribution. The textural properties (surface area, average pore volume and average pore diameter) for natural and calcined calcium/chitosan spheres are reported in Table 3. The calcium/chitosan spheres have no significant surface area: poor textural characteristics. After thermal modification, the average pore volume and pore diameter are much increased: the material has a greater porosity compared to the original material. This result is consistent with SEM observation (Fig. 5). The surface area of calcined calcium/chitosan spheres was compared with the surface area of commercial calcium oxide. The calcined commercial material shows a surface area close to 4–6 $m^2\ g^{-1}$. This means that the use of chitosan as a structuring agent increases the surface area by a factor of about two.[46]

Transesterification reaction

Effect of time

The optimum equilibrium time for the transesterification reaction using the calcined calcium/chitosan spheres was determined by performing the reaction during 9 h. The results show that the conversion of sunflower oil to methyl esters (Y_{FAME}) increases up to 4 h of reaction and then tends to stabilize; the highest conversion of sunflower oil to methyl esters is 52.20 ± 0.08 wt% (Fig. 6). The reaction is reversible, with the highest methyl ester production at 4 h. In the other direction, the production of the reactants (triglycerides) is maximized between 5 and 9 h of reaction, decreasing Y_{FAME}.

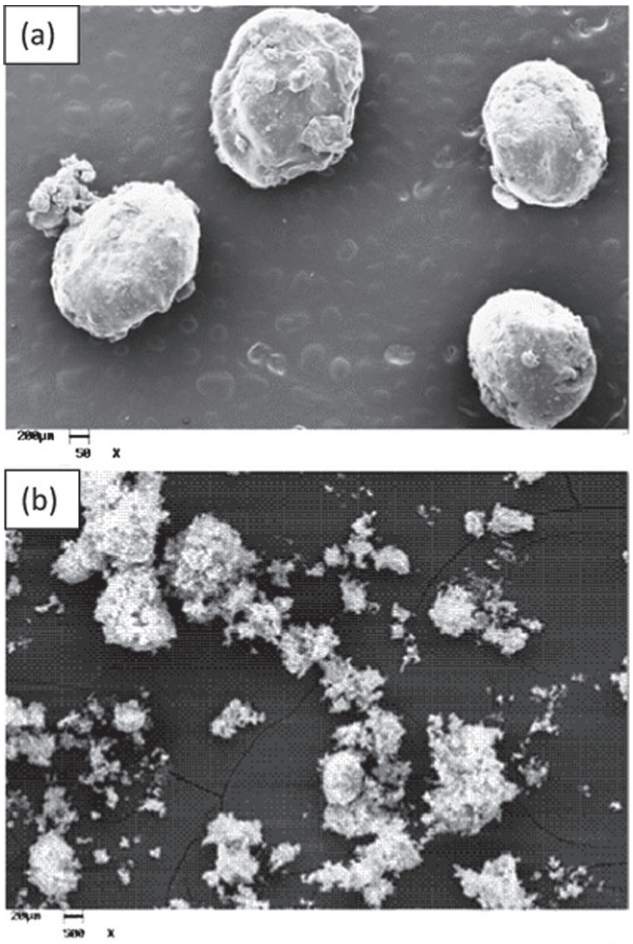

Figure 5. SEM images of (a) calcium/chitosan spheres and (b) calcined calcium/chitosan spheres.

Table 3. Textural properties of materials

Material	S_{BET} [a] ($m^2\ g^{-1}$)	V_p [b] ($cm^3\ g^{-1}$)	D_p [c] (Å)
Calcium/chitosan spheres	0.03	–	–
Calcined calcium/chitosan spheres	11	0.04	138

[a] BET surface area.
[b] Average pore volume.
[c] Average pore diameter.

Experimental design: response surface for conversion of sunflower oil to methyl esters

The results obtained from the experimental design performed under various reaction conditions are reported in Table 4. The response surface plot of the conversion of sunflower oil to methyl esters (Y_{FAME}) as a function of two variables (X_{MR} and X_{CAT}) is shown in Fig. 7. Negative values (−1) on the scale correspond to lower values of the variable and positive values (+1) correspond to higher values of the variable (Table 1). According to the results obtained using the experimental design, the values of Y_{FAME} are higher when using a larger X_{CAT} with a lower X_{MR}.

The molar ratio (X_{MR}) between the reagents is an important variable in the transesterification reaction, since the reaction

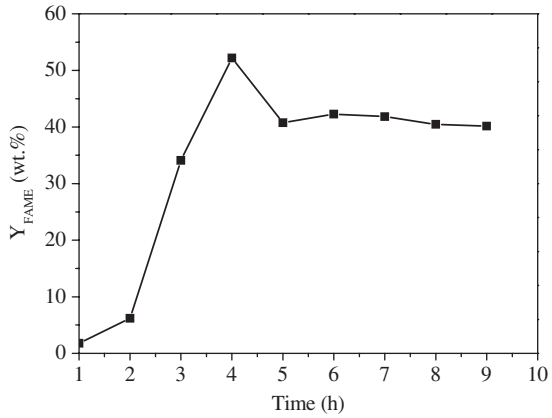

Figure 6. Experimental conditions: X_{MR}, 1:12; X_{CAT}, 3 g (100 g)$^{-1}$; time, 1–9 h; temperature, 60 °C; magnetic stirring, 1000 rpm.

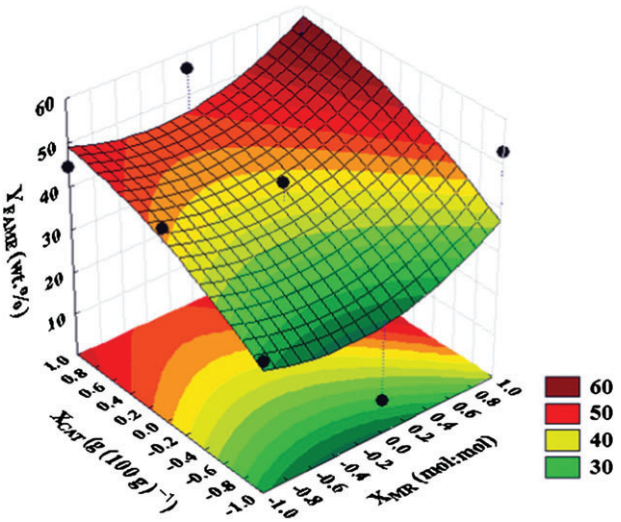

Figure 7. Response surface for the model of calcined calcium/chitosan spheres.

Table 4. Experimental design and results of response surface analysis for conversion of sunflower oil to methyl esters[a]

	Coded variables		Real variables		
Run	X_{MR} (mol/mol)	X_{CAT} (wt%)	X_{MR} (mol/mol)	X_{CAT} (wt%)	Y_{FAME} (wt%)
1	−1	−1	1:6	1	30.64 ± 0.21
2	−1	0	1:6	2	44.97 ± 0.02
3	−1	1	1:6	3	44.72 ± 0.33
4	0	−1	1:9	1	7.81 ± 0.01
5	0	0	1:9	2	43.32 ± 0.05
6	0	1	1:9	3	56.12 ± 0.32
7	1	−1	1:12	1	52.67 ± 0.04
8	1	0	1:12	2	40.54 ± 0.32
9	1	1	1:12	3	52.20 ± 0.20
10	0	0	1:9	2	43.46 ± 0.06
11	0	0	1:9	2	43.38 ± 0.03
12	0	0	1:9	2	43.25 ± 0.12

[a] Data are presented as mean ± standard deviation, $n = 3$.

is reversible. The minimum X_{MR} for producing biodiesel is 1:3. An excess of alcohol over oil is necessary for achieving the complete conversion of sunflower oil to methyl esters. Table 4 shows an increase in the conversion of sunflower oil to methyl esters (Y_{FAME}) with increasing concentration of methyl alcohol in the solution. The maximum conversion of sunflower oil reaches 56.12 ± 0.32 wt% with $X_{MR} = 1{:}9$ and $X_{CAT} = 3$ wt%. This reaction was also conducted using calcined chitosan without calcium as catalyst. This leads to a very low conversion (0.74 ± 0.12%) for the same reaction conditions.

In the case of variable X_{MR}, it is known that excess alcohol in the transesterification reaction shifts the chemical equilibrium of the reaction towards the formation of esters, increasing the conversion. However, the use of a high volume of alcohol complicates the process of gravitational separation between methyl ester and glycerol phases formed, increasing their miscibility and the displacement of the equilibrium favouring the reverse direction (formation of reagents), towards the formation of mono-, di- and triglycerides, thus decreasing the production of methyl esters. This is confirmed by the results obtained for $X_{MR} = 1{:}12$. In addition, an increase in X_{MR} makes more complex the process of separation by gravity between the ester and glycerin phases.

Table 5. Analysis of variance for the conversion of sunflower oil to biodiesel

Source of variation	Sum of squares	Degrees of freedom	Mean square	*F*-value
Regression	1736.23	9	192.91	1.09
Residual	857.53	5	176.50	
Total	2593.10	14		$F_{9,5} = 4.77$

The investigation of the model adjustment was performed by analysis of variance (ANOVA; Table 5). The calculated *F*-value (1.09) is lower than the tabulated $F_{9,5}$ (4.77). Therefore, from the quadratic regression analysis of the results, it is possible to elaborate a model to describe the response variable, Y_{FAME}.

The following equation represents the quadratic model for the studied variables (X_{MR} and X_{CAT}), considering all the regression coefficients for 95% confidence:

$$Y_{FAME}\ (\text{wt}\%) = 40.69 + 4.18X_{MR} + 7.39X_{MR}^2 + 11.08X_{CAT} - 5.68X_{CAT}^2 \quad (2)$$

Equation (2) is valid within the selected experimental range. In other words, the quadratic model obtained cannot be used for predictive purposes (out of the tested range of parameter values).

The response surface analysis is plotted in Fig. 7, confirming that the conversion of the esters decreases at low catalyst concentrations. The most significant factor is X_{CAT}, which has a positive effect on the transesterification reaction. This is due to the fact that an increase in catalyst concentration implies a larger number of active alkaline sites in the reaction medium, which, in turn, increases the conversion of sunflower oil to methyl esters.

Table 6 summarizes some results for biodiesel production using various heterogeneous catalysts. The conversions are higher than those of the present work; however, the reaction conditions are different (higher catalyst amount and oil/alcohol molar ratio). Correia *et al.*[39] used eggshell and crab shell as catalysts and high conversions were observed with the same reaction conditions of

Table 6. Comparison of Y_{FAME} for various catalysts used in transesterification reactions

Oil/alcohol	Catalyst	X_{MR} (mol/mol)	X_{CAT} (g (100 g)$^{-1}$)	Y_{FAME} (wt%)	Ref.
Sunflower oil/methanol	Calcined calcium/chitosan spheres	1:9	3	56.12	This work
Sunflower oil/methanol	Chitosan spheres	1:12	3	0.74	This work
Soybean oil/methanol	Silica-supported tin oxides	1:24	5	81.70	32
Soybean oil/methanol	$Ca_xMg_{2-x}O_2$	1:12	6	91.30	33
Soybean oil/methanol	Immobilized lipase on magnetic chitosan microspheres	1:4	60	87.00	34
Soybean oil/methanol	Calcium-supported tin oxides	1:12	8	89.30	35
Soybean oil/methanol	$CaO-MoO_3$–SBA-15	1:50	6	83.20	36
Soybean oil/methanol	Immobilization of CaO onto chitosan beads	1:13.4	13.78	97.00	12
Sunflower oil/methanol	Eggshell	1:6	3	97.75	39
Sunflower oil/methanol	Crab shell	1:9	3	83.10	39

this study. Experiments should be conducted based on materials with a more dispersed reactive phase, in order to increase the conversion, mechanical resistance and stability.

CONCLUSIONS

Chitosan served as a structural agent in the synthesis of calcium/chitosan spheres. The parameters for the transesterification reaction were optimized using an experimental design method. The results showed that the mixed $CaCO_3$ and CaO have catalytic activity and chitosan particles without calcium are not active for biodiesel production. The main disadvantage in using these materials is in the dispersion of small catalytic particles, which may involve problems in separating the phases at the end of the process. It would probably be important to develop similar materials based on reactive phases. For example, for other applications the materials have been shaped and structured as porous foams. Another possibility, currently under consideration, would be depositing the reactive phases on the surface of structured porous materials (ceramics, carbon, and so on). The structure of these materials is also a criterion apparent to be optimized in order to improve the stability of these supported catalysts, in terms of mechanical resistance and operability.

ACKNOWLEDGEMENTS

The authors acknowledge financial support provided by the Fundação Cearense de Apoio ao Desenvolvimento Científico e Tecnológico (FUNCAP), Conselho Nacional de Desenvolvimento Científico e Tecnológico (CNPq), Coordenação de Aperfeiçoamento de Pessoal de Nível Superior (CAPES) – DGU project 216/12, Bioinorganic Laboratory (UFC-Chemical), X-rays Laboratory (UFC-Physical), Polymer Laboratory (LAPOL, UFC-Chemical), Universidad de Málaga (UMA), and Ministerio de Economia y Competitividad project CTQ 2012-37925-C03-03 and FEDER funds.

SUPPORTING INFORMATION

Supporting information may be found in the online version of this article.

REFERENCES

1 Ma H and Hanna M, *Bioresour Technol* **70**:1–15 (1999).
2 Shahid EM and Jamal Y, *Renew Sust Energy Rev* **12**:2484–2494 (2008).
3 Demirbas A, *Prog Energy Combust Sci* **33**:1–18 (2007).
4 Gerpen JV, *Fuel Process Technol* **86**:1097–1107 (2005).
5 Lotero E, Liu Y, Lopez DE, Suwannakarn K, Bruce DA and Goodwin Jr JG, *Ind Eng Chem Res* **44**:5353–5363 (2005).
6 Kulkarni MG, Dalai AK and Bakhshi NN, *Bioresour Technol* **98**:2027–2033 (2007).
7 Bournay L, Casanave D, Delfort B, Hillion G and Chodorge JA, *Catal Today* **106**:190–192 (2005).
8 Neto PRC, Rossi LFS, Zagonel GF and Ramos LP, *Quím Nova* **23**:531–537 (2000).
9 Watkins RS, Lee AF and Wilson K, *Green Chem* **6**:335–340 (2004).
10 Zhu H, Wu Z, Chen Y, Zhang P, Duan S, Liu X *et al.*, *Chinese J Catal* **27**:391–396 (2007).
11 MacLeod CS, Harvey AP, Lee AF and Wilson K, *Chem Eng J* **135**:63–70 (2008).
12 Fu C-C, Hung T-C, Su C-H, Suryani D, Wu W-T, Dai W-C *et al.*, *Polym Int* **60**:957–962 (2010).
13 Xie W, Huang X and Li H, *Bioresour Technol* **98**:936–939 (2007).
14 Suppes GJ, Dasari MA, Doskocil EJ, Mankidy PJ and Goff MJ, *Appl Catal A* **257**:213–223 (2004).
15 Barakos N, Pasias S and Papayannakos N, *Bioresour Technol* **99**:5037–5042 (2008).
16 Zeng H, Feng Z, Deng X and Li Y, *Fuel* **87**:3071–3076 (2008).
17 Faria EA, Ramalho HF, Marques JS, Suares PAZ and Prado AGS, *Appl Catal A* **338**:72–78 (2008).
18 Long T, Deng Y, Li G, Gan S and Chen Ji, *Fuel Process Technol* **92**:1328–1332 (2011).
19 Lee ST, Mi FL, Shen YL and Shyu SS, *Polymer* **42**:1879–1892 (2001).
20 Roberts GAF, *Chitin Chemistry*. Macmillan Press, London (1992).
21 Leceta I, Guerrero P, Cabezudo S and Caba K, *J Cleaner Prod* **41**:312–318 (2013).
22 Guibal E, *Prog Polym Sci* **30**:71–109 (2005).
23 Sashiwa H and Aiba S-I, *Prog Polym Sci* **29**:887–908 (2009).
24 Guibal E, *Separ Purif Technol* **38**:43–74 (2004).
25 Rabelo RB, Vieira RS, Luna FMT, Guibal E and Beppu MM, *Adsorption Sci Techonol* **30**:1–21 (2012).
26 Agboh OC and Qin T, *Polym Adv Technol* **8**:355–365 (1996).
27 Mi F-L, Shyu S-S, Wu Y-B, Lee S-T, Shyong J-Y and Huang R-N, *Biomaterials* **22**:165–173 (2001).
28 Zabeti M, Daud WMAW and Aroua MK, *Fuel Process Technol* **90**:770–777 (2009).
29 Zabeti M, Daud WMAW and Aroua MK, *Fuel Process Technol* **91**:243–248 (2010).
30 Albuquerque MCG, Jiménez-Urbistondo I, Santamaría-González J, Mérida-Robles JM, Moreno-Tost R, Rodríguez-Castellón E *et al.*, *Appl Catal A* **34**:35–43 (2008).
31 Chun-Chong F, Tien-Chieh H, Chia-Hung S, Devi S, Wen-Teng W, Wei-Chen D *et al.*, *Polym Int* **60**:957–962 (2011).
32 Xie W, Wang H and Li H, *Ind Eng Chem Res* **51**:225–231 (2012).
33 Xie W, Liu Y and Chu H, *Catal Lett* **142**:352–359 (2012).
34 Xie W and Wang J, *Biomass Bioenergy* **36**:373–380 (2012).
35 Xie W and Zhao L, *Energy Convers Manage* **76**:55–62 (2013).
36 Xie W and Zhao L, *Energy Convers Manage* **79**:34–42 (2008).
37 da Silva RB, Neto AFL, dos Santos LSS, Lima JRO, Chaves MH, dos Santos JR Jr *et al.*, *Bioresour Technol* **99**:6793–6798 (2008).

38 Almerindo GI, Probst LFD, Campos CEM, Almeida, RM, Meneghetti SMP, Meneghetti MR *et al.*, *J Power Sources* **196**:8057–8063 (2011).
39 Correia LM, Saboya RMA, Campelo NS, Cecilia JA, Rodríguez-Castellón E, Cavalcante Jr CL *et al.*, *Bioresour Technol* **151**:207–213 (2014).
40 Kayser H, Pienkoß F and de María PD, *Fuel* **116**:267–272 (2014).
41 ISO 15304: Determination of the content of trans fatty acid isomers of vegetables fats and oils. Switzerland (2002).
42 EN 14103: Fat and oil derivatives – Fatty acid methyl esters (FAME) – Determination of ester and linoleic acid methyl ester contents. Switzerland (2003).
43 Antony R, Manickam STD, Saravanan K, Karuppasamy K and Balakumar S, *J Mol Struct* **1050**:53–60 (2013).
44 Přichystalová H, Almonasy N, Abdel-Mohsen AM, Fouda M, Vojtova L, Kobera L *et al.*, *Int J Biol Macromol* **65**:234–240 (2014).
45 Soares AB, Silva PRN, Stumbo AM and Freitas JCC, *Quím Nova* **35**:268–273 (2012).
46 Reyero I, Arzamendi G and Gandía LM, *Chem Eng Res Des* DOI: 10.1016/j.cherd.2013.11.017.